Low-temperature behavior of $YBaCo_2O_{5.5}$: Coexistence of two spin-state ordered phases

D. D. Khalyavin
Institute of Solid State and Semiconductors Physics, National Academy of Sciences, P. Brovka str. 17, 220072 Minsk, Belarus

D. N. Argyriou and U. Amann
Hahn-Meitner-Institut, Glienicker Straße 100, Berlin D-14109, Germany

A. A. Yaremchenko and V. V. Kharton
Department of Ceramics and Glass Engineering, CICECO, University of Aveiro, 3810-193 Aveiro, Portugal
(Received 23 June 2007; published 15 February 2008)

The low temperature antiferromagnetic-antiferromagnetic phase transition in polycrystalline $YBaCo_2O_{5.5}$ cobaltite was studied by neutron powder diffraction. On the basis of symmetry arguments in combination with Rietveld refinement, the coexistence of two phases with different type of spin-state ordering between the diamagnetic ($t_{2g}^6e_g^0$, $S=0$) and paramagnetic ($t_{2g}^4e_g^2$, $S=2$) sixfold coordinated Co^{3+} cations was revealed below the transformation temperature, $T_L \sim 195$ K. One of the phases having *Pmma* ($2a_p \times 2a_p \times 2a_p$) symmetry is characteristic of the high-temperature ($T > T_L$) homogeneous state, whilst another with *Bmmm* ($2a_p \times 2a_p \times 4a_p$) symmetry involves another type of spin-state ordered superstructure. The conjugated magnetic structures possess $\boldsymbol{k}=\boldsymbol{c}^*/2$ and $\boldsymbol{k}=0$ wave vectors, respectively. The structural changes are driven by competition between the elastic and exchange energies.

DOI: 10.1103/PhysRevB.77.064419 PACS number(s): 75.25.+z, 61.05.fm, 61.66.Fn, 71.30.+h

Temperature evolution of the magnetic ground state in $LBaCo_2O_{5.5}$ (L is lanthanide or Y) has attracted great attention in recent years, after discovering their complex behavior related to a succession of the magnetic phase transformations.[1–4] These cobaltites possess also other important properties, particularly giant magnetoresistance[1–4] and high ionic/electronic conductivity.[5,6] At temperatures above $T_{MI} \sim 340$ K, $LBaCo_2O_{5.5}$ and their derivatives exhibit a paramagnetic behavior with metallic-like character of the conductivity. Below T_{MI}, the conductivity decreases rapidly along with substantial crystal structure modifications. In the temperature range T_C (~ 290 K) $< T < T_{MI}$, the magnetic susceptibility still obeys the Curie-Weiss law, but with a considerably smaller effective paramagnetic moment. A long-range magnetic ordering demonstrated by both magnetic measurements[1–4] and neutron diffraction[7–10] occurs below T_C. The latter results in onset of spontaneous magnetization, which is however observed only in a narrow temperature range and disappears at $T_i \sim 260$ K.

This high temperature behavior is qualitatively similar for all cobaltites with different L cations, where the crystal structure involves stripe-type ordering of oxygen ions in the $[LO_{0.5}]$ layers. The ordering results in an orthorhombic *Pmmm* symmetry with the $a_p \times 2a_p \times 2a_p$ unit cell (a_p is the parameter of the pseudocubic perovskite subcell), and provides an alternation of the (ac) plains containing Co^{3+} ions in the octahedral and square-pyramidal coordination. However, the low-temperature magnetic state is different for the cobaltites with relatively small (L=Tb, Dy, and Y) and large (L =Pr, Nd) lanthanide cations. In the former case, the antiferromagnetic structure is changed at $T_L \sim 195$ K.[9,10] When the size of L cations is large, uniform magnetic ordering of the cobalt sublattice is kept in the whole temperature range below T_i.[7,8] The antiferromagnetic-antiferromagnetic phase transition at T_L can only be identified explicitly by neutron diffraction; therefore, the low-temperature magnetic structures of the compounds based on the intermediate lanthanides (L=Sm, Eu, and Gd) having a large neutron absorption cross section cannot be unambiguously discussed at the moment.

The present work is focused on the analysis of the phase transition at T_L in $YBaCo_2O_{5.5}$ cobaltite, which was recently studied by neutron diffraction in the vicinity of antiferromagnetic-ferromagnetic transition at T_i.[10] It has been shown that the latter transformation relates to spin-state ordering phenomenon in the octahedral sublattices of the parent *Pmmm* structure.[10] In the present study, the symmetry arguments were combined with Rietveld analysis to show that the low-temperature neutron diffraction data can be interpreted in terms of two coexisting phases with different types of spin-state ordering and distinct magnetic structures.

The powder of $YBaCo_2O_{5.5}$ used for neutron diffraction and magnetization measurements was prepared by a conventional solid-state reaction technique; detailed description of the synthesis conditions and the oxygen stoichiometry determination by thermogravimetric analysis was published elsewehere.[10] The neutron diffraction experiments were carried out in the Berlin Neutron Scattering Center (BENSC) at the Hahn-Meitner-Institute. Two powder diffractometers were used, namely, the fine-resolution powder diffractometer ($E9$) and the high-intensity flat-cone and powder diffractometer ($E2$). The former, with incident neutrons of wavelength $\lambda = 1.7974$ Å and resolution $\Delta d/d \sim 2 \times 10^{-3}$, was used for the crystal structure refinement. The second diffractometer ($\lambda = 2.39$ Å), equipped with a position-sensitive detector to provide high intensity, is efficient for the magnetic structure investigations. The neutron diffraction patterns were collected on heating after cooling the sample down to 10 K. The Rietveld refinement and group-theoretical calculations were performed using Fullprof suite[11] and ISOTROPY software,[12] respectively.

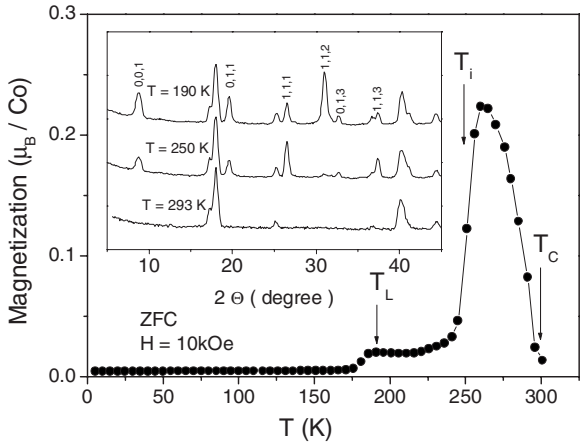

FIG. 1. Temperature dependence of zero field-cooling magnetization registered on heating at $H=10$ kOe. Inset shows the neutron diffraction patterns recorded on the E2 diffractometer, in the paramagnetic region and in the magnetically ordered state above and below T_L. The indexation is given for $2a_p \times 2a_p \times 4a_p$ unit cell.

Figure 1 displays the magnetization curve of $YBaCo_2O_{5.5}$ as a function of temperature. The data was obtained on heating at 10 kOe after cooling the sample in a zero field. Three magnetic phase transformations at $T_L \sim 195$ K, $T_i \sim 260$ K, and $T_C \sim 295$ K can be clearly identified. The neutron diffraction patterns recorded by the $E2$ diffractometer below and above T_L along with the paramagnetic spectrum are presented in the inset. The patterns at 190 K and 250 K can both be indexed in the $2a_p \times 2a_p \times 4a_p$ magnetic unit cell.

The crystal and magnetic structures at $T=250$ K were successfully refined using the models shown in Figs. 2(a) and 2(b), respectively.[10] The crystal structure symmetry is orthorhombic *Pmma* with $2a_p \times 2a_p \times 2a_p$ unit cell. The presence of glide plain perpendicular to the $\boldsymbol{c}$ axis relates to a chessboardlike electronic ordering between the diamagnetic ($t_{2g}^6 e_g^0$) and paramagnetic ($t_{2g}^4 e_g^2$) Co^{3+} ions in the octahedral sublattice. The magnetic structure, with wave vector $\boldsymbol{k}=\boldsymbol{c}^*/2$, clearly provides the antiferromagnetic-ferromagnetic phase transition mechanism at T_i and explains well the metamagnetic behavior below this temperature.[13] However, such model does not allow a satisfactory refinement of the magnetic intensity at low temperatures, $T<T_L$ [Fig. 3(a)].

Plakhty *et al.*[9] pointed out that the $\boldsymbol{k}=\boldsymbol{c}^*/2$ wave vector forbids the presence of the magnetic reflections with $l=2n$. Therefore, at T_L a structural phase transition doubling the $\boldsymbol{c}$ parameter should be involved to resolve the contradiction; in this case, $\boldsymbol{k}=0$ and the $l=2n$ reflections are allowed. These authors[9] proposed the highest *Pcca* subgroup of *Pmma* space group with the modulation vector $\boldsymbol{k}=\boldsymbol{c}^*/2$ for the low-temperature phase. However, taking into account the Wyckoff positions splitting and the distribution of nonequivalent cobalt in the unit cell, this space group was found unlikely.[10] The observation of $(h,0,l,+0,k,l;\ h/k,\ l=2n+1)$ reflections in the recent low-temperature x-ray and neutron diffraction experiments,[14] where the twinned $DyBaCo_2O_{5.5}$ single crystal was studied, also ruled out the *Pcca* symmetry. In the present neutron powder diffraction experiment, detection of these very weak superstructure reflections overlapping with magnetic peaks was practically impossible. Consequently, the methodology developed in Ref. 10 has been applied to deduce the actual symmetry and magnetic structure at low temperatures.

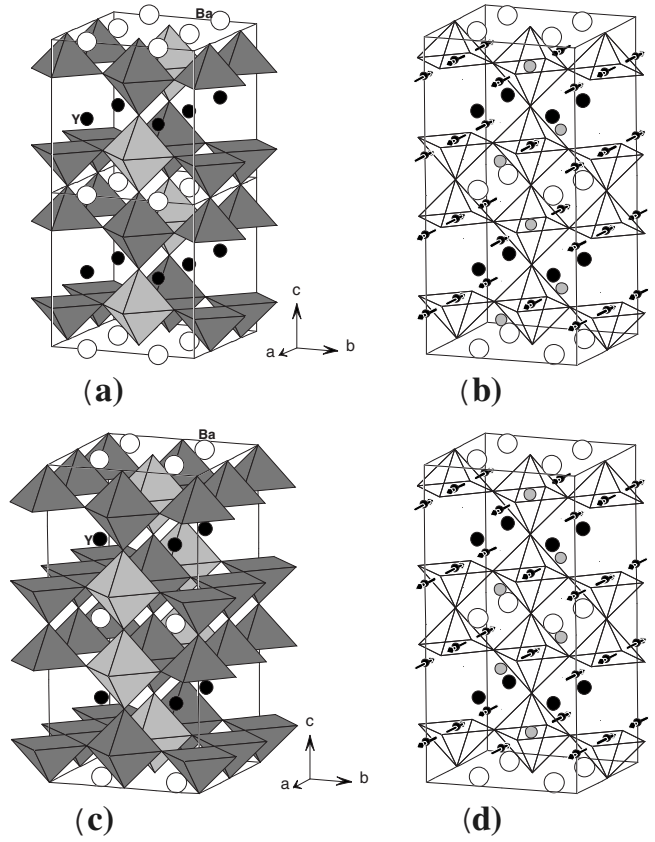

FIG. 2. Schematic representation of the crystal structures with (a) *Pmma* ($2a_p \times 2a_p \times 2a_p$) and (c) *Bmmm* ($2a_p \times 2a_p \times 4a_p$) symmetry, and (b) and (d) the corresponding magnetic structures. Two nonequivalent octahedral Co positions are shown by the light and dark gray polyhedra, respectively. The diamagnetic cobalt ions in the low-spin state are denoted by the gray circles.

The phase transition was suggested to originate from a rearrangement in the $3d$ electronic subsystem of sixfold-coordinated Co^{3+} ions, resulting in a new type of the spin-state ordered superstructure.[10] The appropriate space group should hence correspond to one of the isotropy subgroups of the parent *Pmmm* ($a_p \times 2a_p \times 2a_p$) group, associated with the U ($\boldsymbol{a}^*/2+\boldsymbol{c}^*/2$) point. Two subgroups produced by the U_1^+ and U_2^- irreducible representations split the $2q$ and $2r$ cobalt positions of the parent group, allowing presence of nonequivalent cobalt ions with the same coordination. In both cases, the symmetry is orthorhombic *Cmmm* (or *Bmmm* in nonstandard setting); the lattice vectors with respect to the parent basis are

$$\boldsymbol{a}_s = 2\boldsymbol{c}_p; \boldsymbol{b}_s = 2\boldsymbol{a}_p; \boldsymbol{c}_s = \boldsymbol{b}_p$$

$$(\text{or } \boldsymbol{a}_s = 2\boldsymbol{a}_p; \boldsymbol{b}_s = \boldsymbol{b}_p; \boldsymbol{c}_s = 2\boldsymbol{c}_p$$

$$\text{for the nonstandard setting}),$$

where $\boldsymbol{a}_s$, $\boldsymbol{b}_s$, $\boldsymbol{c}_s$ and $\boldsymbol{a}_p$, $\boldsymbol{b}_p$, $\boldsymbol{c}_p$ are the subgroup and parent-

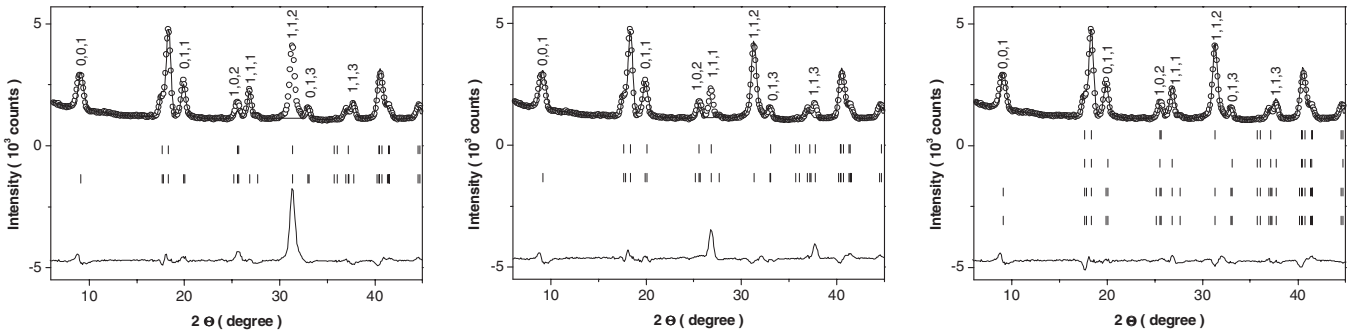

FIG. 3. Neutron powder diffraction data ($E2$ diffractometer, $\lambda = 2.39$ Å) measured at 190 K and refined in different models.

group vectors, respectively. Hereafter, the nonstandard setting is used as the *Bmmm* and *Pmmm* lattice vectors are codirectional.

The location of nonequivalent cobalt sites is the same for both structures ($4h$, $4h$ for octahedral and $4g$, $4g$ for pyramidal); the difference relates to positions occupied by Y and Ba as well as some oxygen positions. The crystal structure associated with the U_1^+ irreducible representation is shown in Fig. 2(c), where the nonequivalent cobalt sites with sixfold coordination are presented by the dark and light polyhedra. The Y and Ba cations are located in the $8m$ and $8n$ positions, respectively. In case of the U_2^- structure, the situation is inverse ($8m$ for Ba and $8n$ for Y, correspondingly).

Following previous results,[10] it seems quite logical to assume that one of the octahedral positions is occupied by diamagnetic low-spin cobalt ions, whereas cobalt in the other sites adopts high-spin configuration. Taking into account the negative exchange interactions between paramagnetic cobalt ions as predicted by the Goodenough-Kanamory rules,[15] the magnetic structure presented in Fig. 2(d) can be easily obtained. The *Pmma* $(2a_p \times 2a_p \times 2a_p) \rightarrow Bmmm$ $(2a_p \times 2a_p \times 4a_p)$ phase transition appears driven by the competition between the elastic and exchange energy, as for the $P4/nmm$ $(3\sqrt{2}a_p \times 3\sqrt{2}a_p \times 2a_p) \rightarrow I4/mmm$ $(3\sqrt{2}a_p \times 3\sqrt{2}a_p \times 4a_p)$ transformation in $YBaCo_2O_{5.44}$.[10] Namely, the sixfold coordinated cobalt ions with nonzero magnetic moment in the high-temperature *Pmma* polymorph are surrounded by four diamagnetic and two paramagnetic neighbours, which is favorable with respect to the elastic energy; in the low temperature *Bmmm* phase, these ions have three diamagnetic and three paramagnetic neighbors, resulting in the exchange energy gain.

The model was preliminary tested to refine the magnetic intensity below T_L. However, this attempt failed [Fig. 3(b)]. The spin configuration presented in Fig. 2(d) provides magnetic contribution to the reflections with $(h,k,l;\ h=2n,\ l=2n+1)$ and $(h,k,l;\ l=2n)$ whereas the magnetic structural factor of the reflections with $(h,k,l;\ h,\ k,\ l=2n+1)$ is zero. All attempts to refine the magnetic structure by other models assuming *Bmmm* symmetry with four independent cobalt positions, were also unsuccessful.

Comparison of the magnetic intensity, calculated for the phase shown in Fig. 2(d), and experimental data makes it possible to conclude that this contribution is superimposed with that of the high-temperature phase. It clearly follows from a comparison of Fig. 3(a) and Fig. 3(b). Indeed, refinement of the low-temperature pattern using the two-phase model was successful, suggesting that a certain fraction of the *Pmma* polymorph exist below T_L [Fig. 3(c)]. Notice that satisfactory results were even obtained when using only two variable parameters; first for the magnetic moments of the pyramidal sublattices and second for the magnetic moments of the high-spin octahedral sublattices, assuming that the cobalt cations with the same coordination have equivalent moments in both phases. The low-spin octahedral sublattices in the phases were fixed to a zero magnetic moment. With these constraints, the fractions of the *Pmma* and *Bmmm* phases at $T = 190$ K were found to be 45.8(5)% and 54.2(5)%, respectively.

The conclusion that below T_L the high temperature polymorph (*Pmma* with the $\boldsymbol{k} = \boldsymbol{c}^*/2$ magnetic wave vector) coexists with the new phase (*Bmmm* with $\boldsymbol{k} = 0$) is in concurrence with recent work by Chernenkov *et al.*[14] The single-

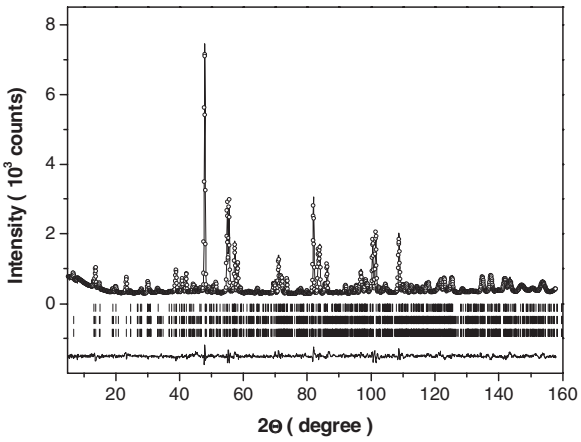

FIG. 4. Neutron powder diffraction data ($E9$ diffractomter, $\lambda = 1.7974$ Å) measured at 10 K. The solid line through the data is the refinement of a model using space group *Bmmm* $(2a_p \times 2a_p \times 4a_p)$. The magnetic scattering was accounted by the two magnetic phases which were modeled by the $2a_p \times 2a_p \times 4a_p$ magnetic unit cell using triclinic P-1 symmetry. It allowed these phases to be appropriately scaled in respect of the single nuclear structure, whereas necessary symmetry constraints were introduced through the codes of the parameters.

crystal neutron diffraction data[14] on $DyBaCo_2O_{5.5}$ coincide with the single-phase model [Fig. 2(d)]; the authors observed sets of the magnetic reflections with $(h,k,l;\ h=2n,\ l=2n+1)$ and $(h,k,l;\ l=2n)$, whilst the reflections with $(h,k,l;\ h,\ k,\ l=2n+1$ were absent below T_L. This indicates that the single crystal does not undergo phase separation below T_L and has *Bmmm* symmetry, thus confirming the relevance of polycrystallinity and microstructural factors. It should be noted that the weak nuclear reflections $(h,0,l+0,k,l;\ h/k,\ l=2n+1)$ observed by Chernenkov *et al.*[14] on the twinned $DyBaCo_2O_{5.5}$ single crystal by x-ray diffraction are consistent with the model proposed in this work, since *Bmmm* space group allows the presence of $(h,0,l)$ reflections with $h+l=2n$. Moreover, since there is no group-subgroup relationship between the *Pmma* and *Bmmm* space groups, the corresponding phase transition should be of the first order, again in agreement with the diffraction experiments.[14]

The crystal structure parameters were determined using the pattern recorded in the high-resolution *E*9 instrument (Fig. 4). The structural parameters were refined in a single phase structural model assuming either *Pmma* (Table I) or *Bmmm* (Table II) symmetry. Unconstrained fitting in the two-phase (*Pmma*+*Bmmm*) model was unstable with slow structure solution oscillations during the least squares refinement. This behavior is not unexpected for the particular case due to negligibly small crystal structure modulations related to the different phases, resulting in a strong correlation between some of the refined parameters. A set of constraints allowed us to reach a convergence, however without a considerable improvement of the refinement quality and the varied structural parameters were very close to those obtained in the corresponding single nuclear phase models. The *Pmma*/*Bmmm* phase ratios deduced from the constrained refinements of the *E*9 diffraction patterns obtained at different temperatures within the $10\ \text{K} < T < 190\ \text{K}$ interval were always very close to 1:1.

The nuclear scattering of the *E*2 patterns was modeled in two-phase structural model with fixed atomic structural parameters. The pattern obtained at 10 K and refined by the two-phase model with the constrained magnetic moments of the pyramidal and octahedral cobalt sublattices as described above is shown in Fig. 5. The phase fractions were found to be very close to those obtained at $T=190$ K being 43.9(5)% for *Pmma* phase and 56.1(5) for *Bmmm* phase. The obtained magnetic moments are 3.2(1) and 2.4(1) μ_B for the octahedral and pyramidal cobalt ions, respectively (they were constrained to be equal in both phases). The former value unambiguously indicates the high-spin electronic configuration, whereas the latter may also be interpreted as intermediate spin-state with additional orbital contribution. However, taking into account the spectroscopic data and theoretical arguments given in Refs. 16 and 17 and the negative exchange interactions with octahedral cobalt, the electronic configuration of the fivefold coordinated Co^{3+} ions should also be high-spin.

Finally, one should consider alternative scenario of the phase transition at T_L, which also involves a reorganization of electronic subsystem of the fivefold-coordinated cobalt ions. Although the high-spin electronic configuration of Co^{3+} was found to be the ground state in the square pyramidal

TABLE I. Atomic positions *x*, *y*, *z*, isotropic temperature factors *B*, and position occupancies, for $YBaCo_2O_{5.5}$ refined in *Pmma* space group from high resolution powder neutron diffraction. The unit cell parameters and reliability factors are $T=190$ K, $a=7.7118(2)$ Å, $b=7.7844(2)$ Å, $c=7.4915(2)$ Å, $R_p=5.81\%$, $R_{wp}=7.39\%$, $\chi^2=2.64$; $T=75$ K, $a=7.7091(2)$ Å, $b=7.7761(2)$ Å, $c=7.4863(2)$ Å, $R_p=6.60\%$, $R_{wp}=8.36\%$, $\chi^2=2.24$; $T=10$ K, $a=7.7075(2)$ Å, $b=7.7718(2)$ Å, $c=7.4840(2)$ Å, $R_p=6.93\%$, $R_{wp}=8.76\%$, $\chi^2=2.45$.

T		190 K				75 K				10 K				
Atom	Wyck	x	y	z	B	Occup.	x	y	z	B	Occup.	x	y	z	B	Occup.
Y	4*h*	0	0.2711(7)	0.5	0.87(8)	1	0	0.2703(7)	0.5	0.56(9)	1	0	0.2694(7)	0.5	0.37(8)	1
Ba	4*g*	0	0.250(1)	0	0.5(1)	1	0	0.249(1)	0	−0.1(1)	1	0	0.250(1)	0	0.0(1)	1
Co_{Py1}	2*e*	0.25	0	0.259(2)	0.8(1)	1	0.25	0	0.259(2)	0.5(1)	1	0.25	0	0.260(2)	0.4(1)	1
Co_{Py2}	2*e*	0.25	0	−0.259(2)	0.8(1)	1	0.25	0	−0.259(2)	0.5(1)	1	0.25	0	-0.260(2)	0.4(1)	1
Co_{Oc1}	2*f*	0.25	0.5	0.249(2)	0.8(1)	1	0.25	0.5	0.247(2)	0.5(1)	1	0.25	0.5	0.247(2)	0.4(1)	1
Co_{Oc2}	2*f*	0.25	0.5	−0.249(2)	0.8(1)	1	0.25	0.5	−0.247(2)	0.5(1)	1	0.25	0.5	-0.247(2)	0.4(1)	1
O1	2*e*	0.25	0	−0.002(3)	0.9(2)	1	0.25	0	−0.003(5)	1.0(2)	1	0.25	0	−0.008(3)	0.5(2)	1
O2	4*i*	0.015(2)	0	0.3122(9)	1.1(2)	1	0.015(2)	0	0.3121(9)	0.9(2)	1	0.019(2)	0	0.313(1)	0.4(1)	1
O3	4*k*	0.25	−0.231(1)	−0.301(2)	0.5(3)	1	0.25	−0.231(1)	−0.299(2)	0.4(3)	1	0.25	−0.231(1)	−0.303(2)	0.5(2)	1
O4	4*k*	0.25	0.255(1)	0.299(2)	1.1(3)	1	0.25	0.254(1)	0.303(2)	0.7(3)	1	0.25	0.255(1)	0.297(2)	0.4(2)	1
O5	2*f*	0.25	0.5	−0.004(4)	0.9(2)	1	0.25	0.5	0.007(4)	0.7(2)	1	0.25	0.5	0.005(4)	0.7(2)	1
O6	4*j*	−0.008(3)	0.5	0.266(1)	2.3(2)	1	−0.011(3)	0.5	0.266(1)	2.1(2)	1	−0.010(2)	0.5	0.267(1)	2.2(2)	1
O7	2*f*	0.25	0.5	0.498(4)	1.9(3)	0.90(2)	0.25	0.5	0.494(5)	1.7(3)	0.91(2)	0.25	0.5	0.494(4)	2.0(3)	0.94(2)
O71	2*e*	0.25	0	0.5	0(–)	0.02(2)	0.25	0	0.5	0(–)	0.00(2)	0.25	0	0.5	0(–)	0.00(2)

TABLE II. Atomic positions x, y, z, isotropic temperature factors B, and position occupancies, for $YBaCo_2O_{5.5}$ refined in the *Bmmm* space group from the high resolution powder neutron diffraction. The unit cell parameters and reliability factors are $T=190$ K, $a=7.7118(2)$ Å, $b=7.7844(2)$ Å, $c=14.9823(4)$ Å, $R_p=5.98\%$, $R_{wp}=7.64\%$, $\chi^2=2.76$; $T=75$ K, $a=7.7091(2)$ Å, $b=7.7760(2)$ Å, $c=14.9718(6)$ Å, $R_p=6.79\%$, $R_{wp}=8.65\%$, $\chi^2=2.4$; $T=10$ K, $a=7.7075(2)$ Å, $b=7.7717(2)$ Å, $c=14.9673(6)$ Å, $R_p=7.11\%$, $R_{wp}=9.14\%$, $\chi^2=2.66$.

T		190 K					75 K					10 K					
Atom	Wyck	x	y	z	B	Occup.	x	y	z	B	Occup.	x	y	z	B	Occup.
Y	8*m*	0.25	0.2719(6)	0.25	0.77(8)	1	0.25	0.2705(7)	0.25	0.5(1)	1	0.25	0.2702(7)	0.25	0.24(9)	1
Ba	8*n*	−0.752(4)	0.2489(9)	0	0.1(1)	1	−0.747(3)	0.248(1)	0	0.0(1)	1	−0.746(3)	0.249(1)	0.5	−0.1(1)	1
Co_{Py1}	4*g*	0	0	0.1296(9)	0.6(1)	1	0	0	0.1299(9)	0.3(1)	1	0	0	0.130(1)	0.2(1)	1
Co_{Py2}	4*g*	0	0	0.6296(9)	0.6(1)	1	0	0	0.6299(9)	0.3(1)	1	0	0	0.630(1)	0.2(1)	1
Co_{Oc1}	4*h*	0	0.5	0.1241(9)	0.6(1)	1	0	0.5	0.1232(9)	0.3(1)	1	0	0.5	0.123(1)	0.2(1)	1
Co_{Oc2}	4*h*	0	0.5	0.6241(9)	0.6(1)	1	0	0.5	0.6232(9)	0.3(1)	1	0	0.5	0.623(1)	0.2(1)	1
O1	2*a*	0	0	0	1.6(9)[a]	1	0	0	0	2.3(9)[a]	1	0	0	0	1.4(8)[a]	1
O2	2*b*	0	0	0.5	0.4(6)[a]	1	0	0	0.5	−0.2(5)[a]	1	0	0	0.5	0.4(6)[a]	1
O3	2*d*	0	0.5	0	1.2(9)[a]	1	0	0.5	0	2.0(8)[a]	1	0	0.5	0	1.4(7)[a]	1
O4	2*c*	0	0.5	0.5	0.4(9)[a]	1	0	0.5	0.5	−0.3(9)[a]	1	0	0.5	0.5	−0.5(9)[a]	1
O5	8*p*	−0.260(2)	0	0.6559(5)	1.0(3)	1	−0.260(2)	0	0.6556(5)	0.7(2)	1	−0.267(2)	0	0.6563(5)	0.3(2)	1
O6	8*q*	−0.250(5)	0.5	0.6328(6)	2.3(2)	1	−0.252(4)	0.5	0.6329(6)	2.2(2)	1	−0.249(3)	0.5	0.6334(6)	2.1(2)	1
O7	8*o*	0	0.240(3)	0.151(2)	1.3(3)	1	0	0.247(2)	0.152(1)	0.8(3)	1	0	0.240(2)	0.152(1)	0.6(3)	1
O8	8*o*	0	0.240(2)	0.650(2)	0.5(3)	1	0	0.235(1)	0.649(1)	0.4(3)	1	0	0.243(2)	0.648(1)	0.4(3)	1
O9	4*h*	0	0.5	0.250(3)	1.8(3)	0.90(2)	0	0.5	0.251(3)	1.5(3)	0.91(2)	0	0.5	0.249(3)	2.0(3)	0.95(2)
O91	4*g*	0	0	0.25(-)	0(–)	0.01(2)	0	0	0.25(-)	0(–)	0.00(2)	0	0	0.25(-)	0(–)	0.00(2)

[a]1*a* and 1*e* oxygen positions of the parent *Pmmm* space group are split in the *Bmmm* subgroup in to 2*a*, 2*b* and 2*d*, 2*c*, respectively, resulting in their low statistic weight and consequently large standard deviations for variable parameters related to these positions.

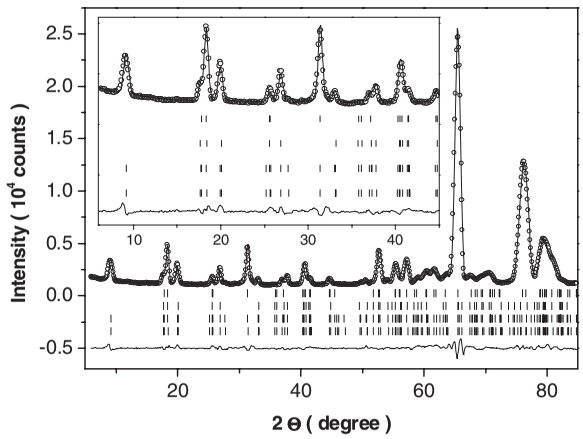

FIG. 5. Neutron powder diffraction data (*E*2 diffractomter, λ =2.39 Å) measured at 10 K. The solid line represents the refinement of the two-phase model described in the text. Inset shows an expanded portion in the 2Θ range 10–45°. $R_{nuc(Pmma)}=4.43\%$, $R_{nuc(Bmmm)}=4.13\%$, $R_{mug(Pmma)}=13.9\%$, and $R_{mug(Bmmm)}=10.8\%$.

coordination, the phase transition may involve charge disproportionation. In other words, if the average oxidation states of the pyramidal and octahedral sublattices are different, charge ordering below T_L may also change the symmetry and magnetic structure. As the refinement of magnetic structure using a single-phase model with four independent cobalt positions was unsuccessful for both *Pmma* ($2a_p\times 2a_p\times 2a_p$) and *Bmmm* ($2a_p\times 2a_p\times 4a_p$) space groups, one possible situation may appear when 2*r* (octahedral) and 2*q* (pyramidal) positions in the parent *Pmmm* ($a_p\times 2a_p\times 2a_p$) group are split by irreducible representations associated with different $\boldsymbol{k}$ points. In order to obtain appropriate subgroups with the $2a_p\times 2a_p\times 4a_p$ unit cell dimension, combinations of the irreducible representations splitting the 2*r* and 2*q* positions and associated with the $X(\boldsymbol{k}=\boldsymbol{a}^*/2)$, $Z(\boldsymbol{k}=\boldsymbol{c}^*/2)$, and $U(\boldsymbol{k}=\boldsymbol{a}^*/2+\boldsymbol{c}^*/2)$ points should be analyzed. Consequently, the coupled subgroups produced by the reducible representations $X_2^-\oplus Z_1^+$, $X_2^-\oplus Z_2^-$, $X_2^-\oplus U_1^+$, and $X_2^-\oplus U_2^-$, were calculated. In all cases, the resultant symmetry is *Pmma* ($2a_p\times 2a_p\times 4a_p$)

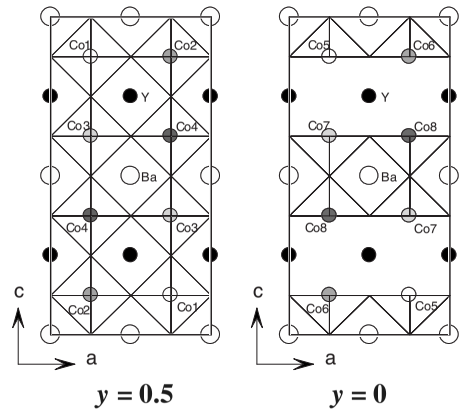

FIG. 6. Distribution of nonequivalent octahedral and pyramidal cobalt in the $2a_p\times 2a_p\times 4a_p$ supercell for the *Pmma* isotropy subgroup produced by $X_2^-\oplus U_1^+$ reducible representation.

with eight independent cobalt positions in the unit cell (Fig. 6). The magnetic structure refinement was then attempted using a single-phase model involving eight independent cobalt spins. However, although the number of variables was large enough, no satisfactory solution was found.

In conclusion, polycrystalline $YBaCo_2O_{5.5}$ exhibits structural changes at $T_L \sim 195$ K. Above this temperature, the crystal structure is orthorhombic *Pmma* $(2a_p \times 2a_p \times 2a_p)$ with chessboardlike spin-state ordering between the low- and high-spin Co^{3+} cations in the octahedral sublattice. This type of superstructure is favorable in terms of the elastic energy; the magnetic structure wave vector is $\boldsymbol{k}=\boldsymbol{c}^*/2$. Below T_L, the *Pmma* phase coexists with another orthorhombic *Bmmm* $(2a_p \times 2a_p \times 4a_p)$ phase, where the type of spin-state ordering between the diamagnetic and paramagnetic octahedrally coordinated Co^{3+} ions is different. The phase ratio, close to 1:1 at $T=190$ K, was found essentially temperature-independent. The different type of electronic ordering leads to a change in the magnetic structure. The conjugated spin-ordered configuration has the wave vector $\boldsymbol{k}=0$ and is favorable with respect to the exchange energy.

The neutron diffraction experiment at BENSC was supported by the European Commission under the 6th Framework Programme through the Key Action: Strengthening the European Research Area, Research Infrastructures, Contract No. RII3-CT-2003-505925 (NMI3).

[1] C. Martin, A. Maignan, D. Pelloquin, N. Nguyen, and B. Raveau, Appl. Phys. Lett. **71**, 1421 (1997).
[2] I. O. Troyanchuk, N. V. Kasper, D. D. Khalyavin, H. Szymczak, R. Szymczak, and M. Baran, Phys. Rev. Lett. **80**, 3380 (1998).
[3] I. O. Troyanchuk, N. V. Kasper, D. D. Khalyavin, H. Szymczak, R. Szymczak, and M. Baran, Phys. Rev. B **58**, 2418 (1998).
[4] A. Maignan, C. Martin, D. Pelloquin, N. Nguyen, and B. Raveau, J. Solid State Chem. **142**, 247 (1999).
[5] A. A. Taskin, A. N. Lavrov, and Y. Ando, Appl. Phys. Lett. **86**, 091910 (2005).
[6] G. Kim, S. Wang, A. J. Jacobson, Z. Yuan, W. Donner, C. L. Chen, L. Reimus, P. Brodersen, and C. A. Mims, Appl. Phys. Lett. **88**, 024103 (2006).
[7] F. Fauth, E. Suard, V. Caignaert, and I. Mirebeau, Phys. Rev. B **66**, 184421 (2002).
[8] C. Frontera, J. L. Garcia-Munoz, A. E. Carrillo, M. A. G. Aranda, I. Margiolaki, and A. Caneiro, Phys. Rev. B **74**, 054406 (2006).
[9] V. P. Plakhty, Y. P. Chernenkov, S. N. Barilo, A. Podlesnyak, E. Pomjakushina, E. V. Moskvin, and S. V. Gavrilov, Phys. Rev. B **71**, 214407 (2005).
[10] D. D. Khalyavin, D. N. Argyriou, U. Amann, A. A. Yaremchenko, and V. V. Kharton, Phys. Rev. B **75**, 134407 (2007).
[11] J. Rodriguez-Carvajal, Physica B **192**, 55 (1993).
[12] H. T. Stokes and D. M. Hatch, ISOTROPY, 2002, http://stokes.byu.edu/isotropy.html
[13] D. D. Khalyavin, Phys. Rev. B **72**, 134408 (2005).
[14] Yu. P. Chernenkov, V. P. Plakhty, A. G. Gukasov, S. N. Barilo, S. V. Shiryaev, G. L. Bychkov, V. Hinkov, V. I. Fedorov, and V. A. Chekanov, Phys. Lett. A **365**, 166 (2007).
[15] J. B. Goodenough, *Magnetism and the Chemical Bond* (Interscience, New York, 1963).
[16] Z. Hu, H. Wu, M. W. Haverkort, H. H. Hsieh, H. J. Lin, T. Lorenz, J. Baier, A. Reichl, I. Bonn, C. Felser, A. Tanaka, C. T. Chen, and L. H. Tjeng, Phys. Rev. Lett. **92**, 207402 (2004).
[17] W. R. Flavell, A. G. Thomas, D. Tsoutsou, A. K. Mallick, M. North, E. A. Seddon, C. Cacho, A. E. R. Malins, S. Patel, R. L. Stockbauer, R. L. Kurtz, P. T. Sprunger, S. N. Barilo, S. V. Shiryaev, and G. L. Bychkov, Phys. Rev. B **70**, 224427 (2004).